A NEBULIZER SYSTEM FOR POSITRON EMISSION TOMOGRAPHY IMAGING OF AEROSOLS AND NANOPARTICLES FOR USE IN PRECLINICAL PULMONARY DRUG DELIVERY STUDIES

An Undergraduate Research Scholars Thesis

by

ANDREW STERLING BUTTERS

Submitted to the Undergraduate Research Scholars program at
Texas A&M University
in partial fulfillment of the requirements for the designation as an

UNDERGRADUATE RESEARCH SCHOLAR

Approved by Research Advisor: Dr. Gamal Akabani

May 2017

Major: Nuclear Engineering

TABLE OF CONTENTS

Page

ABSTRACT 1

ACKNOWLEDGMENTS 3

NOMENCLATURE 4

CHAPTER

I. INTRODUCTION 5

Overview 5
Merit in Nebulizer Therapy 6
Theory & Existing Work 7

II. DEVICE DESIGN AND FEATURES 16

Overview 16
Bruker Albira Si 17
Integration 18
Atomizer/Nebulizer 19
Anesthesia System 20
Mixing Chamber 21
Exhaust Vacuum System 22
Physiological Monitoring System 23
Isolation System 23
General 24

III. METHODOLOGY 25

Fluid Dynamics 25
MPPD Calculations 25
System Integration & Characterization 27

IV. RESULTS AND DISCUSSION 29

V. CONCLUSION 31

REFERENCES 33

APPENDIX 37

ABSTRACT

A Nebulizer System for Positron Emission Tomography Imaging of Aerosols and Nanoparticles for Use in Preclinical Pulmonary Drug Delivery Studies

Andrew Sterling Butters
Department of Nuclear Engineering
Texas A&M University

Research Advisor: Dr. Gamal Akabani
Department of Nuclear Engineering
Texas A&M University

This research project proposes to develop, integrate and characterize a nebulizer system for the nasal pulmonary delivery of radiopharmaceuticals in the form of aerosols containing nanoparticles for dynamic imaging studies using positron emission tomography (PET) in small animal models of disease. PET imaging of inhaled radiolabeled drugs in the form of aerosols containing nanoparticles can provide an in vivo measurement of drug distribution using the drug itself as the tracer. The system will be composed of 1) a nebulizer generator, 2) an anesthesia system, 3) a gas exhaust system, 4) a physiological monitoring system for respiratory synchronization and nebulizer triggering, and 5) a cylindrical bed to house in isolation the rodent. The proposed nebulizer system will be integrated into the Albira Si micro-PET/SPECT/CT imaging unit and it will help carry out translational imaging studies of novel PET radiolabeled drugs in small animal models of lung disease, such as lung cancer. The nebulizer system will be integrated and characterized for activity median aerodynamic diameter (AMAD) particle size distribution, aerosol mass distribution, nebulizer triggering using the

respiratory cycle, drug and activity pulmonary distribution, and inhalation fraction and particle distribution in a normal and diseased rodent's lung model.

ACKNOWLEDGEMENTS

I would like to thank my Principal Investigator and professor, Dr. Gamal Akabani, and Ryan Clanton, for their guidance and support throughout the course of this research.

Thanks also goes to the Undergraduate Research Scholars Program for assistance in the synthesis of this document and guidance along the way.

NOMENCLATURE

PET	Positron Emission Tomography
SPECT	Single-Photon Emission Computed Tomography
CT	Computed Tomography
NP	Nanoparticle
MPPD	Multiple-Path Particle Dosimetry Model
IRV	Inspiratory Reserve Volume
IC	Inspiratory Capacity
VC	Vital Capacity
FRC	Functional Residual Capacity
ERV	Expiratory Reserve Volume
RV	Residual Volume
TLC	Total Lung Capacity
SLC	Solute Carrier (transporter)
ABC	ATP-Binding Cassette (transporter)
FRC	Functional Residual Capacity
GSD	Geometric Standard Deviation
MMAD	Mass Median Aerodynamic Diameter
TNF-α	Tumor Necrosis Factor Alpha
^{18}FDG	Fludeoxyglucose (^{18}F)

CHAPTER I

INTRODUCTION

Overview

In vivo imaging is an important tool for preclinical studies of lung function and disease. The widespread availability of multimodal animal imaging systems and the rapid rate of improvement of diagnostic contrast agents have allowed researchers to noninvasively study lung function and pulmonary disorders [1]. There are several imaging modalities used in molecular imaging, these are planar x-ray, computerized tomography (CT), magnetic resonance imaging (MRI), single photon emission tomography (SPECT), positron emission tomography (PET/CT), and bioluminescence [2-4]. All these modalities have their advantages and limitations. Using any one of the above imaging modalities it is possible to diagnose, track, and quantify biological processes over time. The use of bioluminescence, fluorescence, planar x-ray, x-ray computed tomography, magnetic resonance imaging, and nuclear imaging modalities (positron emission tomography and single photon emission computed tomography) for the study of lung function and pulmonary disorders have been employed in the preclinical setting [5]. However, the diagnosis and therapy of lung diseases continuous to be problematic [6-10]. The direct delivery of drugs to the lungs is a difficult task that requires the merging of engineering principles in aerosol sciences and molecular imaging, including the sustained drug release after inhalation [11-15].

Merit in Nebulizer Therapy

Therapies for lung diseases have improved with the development of new highly efficient nebulizers that can produce quasi-monodisperse aerosols capable of penetrating the deepest regions of the lung [15]. However, the use and reporting of nebulizers is often inconsistent and many research studies are irreproducible. Therefore, the standardization of the these devices provides researchers the capacity to reproduce studies and duplicate the consistent delivery of aerosols to patients [16]. Furthermore, with the advent of active biological nanoparticles as drugs, this delivery method is being further investigated to characterize the delivery, pharmacokinetics, pharmacodynamics, and overall safety and efficacy of nanoparticles in the form of aerosols [17, 18]. However, the study of these aerosol and nanoparticle based drugs requires that preclinical animal models be used to assess their safety and efficacy as per FDA guidelines. FDA regulates nanotechnology products under existing statutory authorities, in accordance with the specific legal standards applicable to each type of product under its jurisdiction [19]. We consider the current framework for safety assessment sufficiently robust and flexible to be appropriate for a variety of materials, including nanomaterials. FDA maintains a product-focused, science-based regulatory policy. Technical assessments will be product-specific, taking into account the effects of nanomaterials in the particular biological and mechanical context of each product and its intended use" [19]. One product, Aurimune (CYT-6091) by CytImmune Sciences, Inc utilizes colloidal gold and is approved for Phase II Preclinical studies for solid tumors using TNF-α targeting mechanism [20, 21]. The proposed system will help develop translational physiologically based pharmacokinetic models of radiolabeled, functionalized gold nanoparticle aerosols inhaled by animal models of disease, which in turn can help develop therapy strategies for those in humans.

Theory & Existing Work

This research is comprised of several areas of design and experimentation. These areas will be explored to develop a methodology that will assist in providing consistency in the results of research. There are two areas of interest: therapeutic pulmonary delivery in rodents and the behavior of aerosols in the lungs.

The Vibrating Mesh Atomizer

This device consists of an annular piezoelectric element that surrounds and contacts the mesh. The mesh consists of thousands of holes possessing a conical structure. The larger cross-section of this conical structure faces the fluid supply for loading. As the piezoelectric element activates, it produces a vibration in the mesh that deforms into the fluid supply thus ejecting a population of fluid particles on the opposite side. “They have silent operation, short treatment times, increased output efficiency, and minimal residual volume. Advantages of mesh nebulizers include consistent and improved aerosol generation efficiency, a predominantly ne-particle fraction reaching into the peripheral lung, low residual volume, and the ability to nebulize in low drug volumes. The size of the pore, the aerosol chamber, and the reservoir, as well as the output rate of mesh nebulizers, can be adjusted for different drugs to optimize aerosol drug delivery to patients. Mesh nebulizers are more efficient than jet nebulizers and can provide higher drug doses to patients. Although human studies with mesh nebulizers are limited, in vitro studies demonstrated approximately 2-3 times higher lung deposition with mesh nebulizers when compared to jet nebulizers” [22-25]. It is important to consider, though, that the aerosol output rate and inhaled fraction will be largely influenced by drug formulations. That is, the

performance of these vibrating mesh nebulizers can be hindered by suspensions with a high surface tension. In addition, reports exist regarding the blockage of the mesh perforations [26].

Aerosol Characterization

Several characterization techniques and attributes exist for a thorough depiction of an aerosol and its predicted behavior. One of the key characteristics is known as aerodynamic diameter. It is defined as the equivalent diameter of a spherical particle with specific gravity unit density but the same settling velocity as the particle under scrutiny. By formulating this attribute, one can account for the particle aspect ratio, shape, and size of an individual particle. Since aerosols are the sum combination of a large population of particles, the population is described using the mass median aerodynamic diameter expressed using geometric standard deviation. The geometric standard deviation threshold between mono and poly-dispersed particles is taken to be 1.0 - 1.2 where particle populations above this threshold are considered poly-dispersed.

Humans vs Mice

Inhalation is the most significant exposure route for airborne nanoparticles [27]. In mammals, the respiratory system can be partitioned into several regions: extra thoracic/nasopharyngeal region (nose, mouth, pharynx, larynx), tracheobronchial region (trachea to terminal bronchioles: main bronchus, lobar bronchus, segmental bronchus, sub-segmental bronchus, conducting bronchiole), and the pulmonary/alveolar region (respiratory bronchiole, alveolar duct, alveolar sac, alveolus). A descent into the lungs instigates several trends: an increase in the generation of branching, total cross-sectional area, and the residence time in the airway; a decrease in the diameter and length of the airway, velocity of fluid in the airway. The

relationship that exists between these trends is as follows: the length/diameter decrease and branching number increase intuitively elicits a reduction in velocity and increase in residence time. These trends distinctly characterize each airway in the lungs thus aerosol particle deposition and subsequent deposition mechanisms are also distinct per location in the lung.

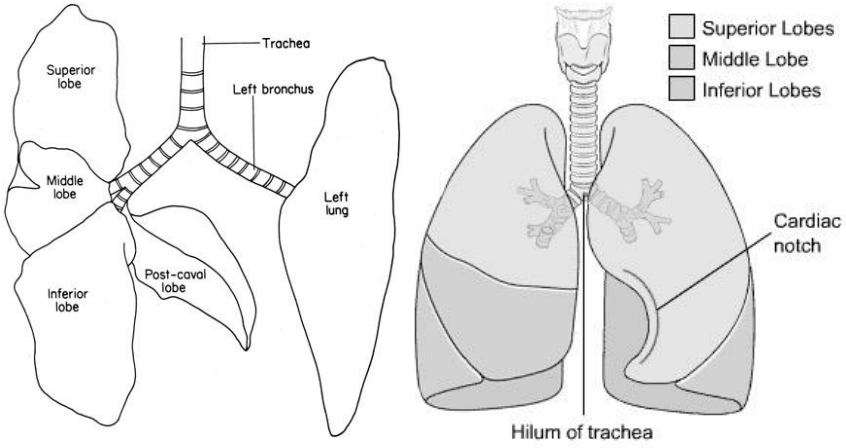

Figure 1. Comparison of the human (right) and mice (left) lung. Adapted from [28].

There are many important considerations regarding the differences between human and murine lungs [29-31]. The total lung capacity (TLC) of the mouse is about 1 ml compared to 6,000 ml of a human. Both humans and mice have 5 lobes distributed between both lungs however the left lung in mice is composed of a single lobe. The mouse lung parenchyma occupies 18% of the total lung compared to that of 12% for a human. The alveoli of the mouse lung have a mean linear intercept of 80 μm compared to that of 210 μm for a human thus they are significantly smaller. The blood-gas barrier thickness in the mouse is 0.32 μm compared to that of 0.62 μm for a human, which might have important implications for gas exchange, parenchymal lung mechanics, and nanoparticle translocation. Fewer respiratory bronchioles and airway generations (13–17 generations) oppose the more numerous (17–21 generations) of the

human lung. The lungs of each species also differ in symmetry: a monopodial branching pattern for mice in contrast to a dichotomous branching pattern for humans. Mice also possess a relatively large airway lumen compared to humans [32]. The relatively large size of the lumen in mice is likely in place to accommodate air resistivity induced by the rapid respiratory rate (250 – 350 bpm) required to maintain body temperature [31]. The distribution of submucosal glands is different than that seen in humans, present only in the trachea [33]. Lastly, mice tend to have a large number of Clara cells [30]. These are morphologically distinct cells that have identified importance in anatomical fortification against environmental exposures [36]. In summary, there a greater number of differences between the lungs of these species and not all have been detailed here. In addition, not only do geometrical differences exist between human and murine lungs, but also pathological, physiological, and histological differences as well. The symmetry and size of the branching in the lungs will comprise most geometrical differences. These geometrical differences and some physiological differences will affect the deposition of aerosols in the lungs of each species. The more complex pathological, physiological, and histological differences will affect the nature of tumor formation and response to aerosolized nanoparticles in both species which may be an important consideration for therapeutic treatment. With xenografting, genetic lesions of human lung cancer have been introduced into murine pulmonary tissue to yield lung tumors with similar characteristics to those found in humans. In addition, transgenic models have allowed for the assessment of oncogenes in tumor origination and development by focusing their expression in a subset of lung epithelial cells [5, 34]. The superiority of xenograft, transgenic, syngeneic (limited to Lewis lung carcinoma model), and spontaneous tumor models is debatable; however, the use of these models has provided a significant advancements in preclinical studies in spite of lack of reliability [35]. Murine models possess many advantages, though, to include

human genome similarity, proven successful validation of drug target and dosage schemes, cost-effectiveness and reproducibility, and large–scale phenotyping [36].

Nanoparticle Synthesis, Radiolabeling, Functionalization, and Translocation

Several methods exist for synthesizing gold NPs. At the most basic level, they are produced via the reduction of chloroauric acid $H[AuCl_4]$. The Turkevich method is the simplest method available and produces gold nanoparticles suspended in water that are around 10-20 nm with the normally desired spherical shape and monodispersity. Production of larger particles may not yield these desirable characteristics. The Brust method is used to produce gold nanoparticles in organic liquids that are not miscible with water that will be in the 2 – 6 nm range. The Martin method using a $NaBH_4$ reducing agent and produces nanoparticles in the 3.2 – 5.2 nm range which are comparable to those produced using the Brust method. Sonolysis is another method that utilizes ultrasound in the presence of chlorauric acid and glucose to form 30 – 50 nm nanoribbons. Spherical nanoparticles can be synthesized using this technique by substituting glucose with cyclodextrin. Many colloidal nanoparticle synthesis methods have been documented and characterized [44]. Radiolabeled gold nanoparticles can be created by using ^{198}Au for the nanoparticle synthesis. This isotope is a beta emitter with a range in tissue of about 11 mm and half-life of 2.7 days. It is also speculated that these gold nanoparticles can be synthesized in such a way that they can contain a variety of radioactive isotopes. This serves the purpose of flexibility in treatments based on the properties of the isotope: half-life, decay mode, decay emission range, etc. Nanoparticle deposition and fate appears understood in a variety of scenarios upon a variety of criteria [28]. PEGylation has emerged as a strategy to enhance solubility of hydrophobic drugs, prolong circulation time, minimize non-specific uptake, and

allow for specific tumor-targeting through the enhanced permeability and retention effect [46]. The process consists of coating the nanoparticle with polyethylene glycol. Nanoparticle retention is thus extended due to prolonged circulation time. This extension in retention is achieved by mitigating the aggregation of nanoparticles in organs and phagocytosis by the reticuloendothelial system due to the inherent response toward PEG. This response is achieved by passivating the nanoparticle surface so as to conceal the surface reactivity of the nanoparticle. The difference in response has been shown between PEGylated and non-PEGylated nanoparticles [47]. An excellent article has been published that is very similar to the objective of this study [48]. However, the strategy outlined in this study did not include PEGylation or other functionalization strategies. Attaching targeting moieties on PEGylated nanoparticles further enhances their targeting of tumors [49-51]. This has been proven in several studies. Glucose is a common SLC transport system of which there are over 400 members. Glucose is actually the transport system of FDG [53]. Maltodextrin is similar to dextrose (glucose) in absorption properties however some studies have reported possible elevated absorption rates when comparing glucose and maltodextrin diets [54]. This projection of elevated absorption rates makes maltodextrin a more attractive candidate as a transport system. In summary, it is intended the nanoparticles

Clearance Mechanisms

Following deposition, the presence of particles is portrayed in two regards: retention and clearance. Retention, as the name suggests, is the tendency of particles to remain in pulmonary airways. Retention is dependent upon the particle physiochemical properties, the location of their deposition, and the clearance mechanism involved. Contrary to retention, clearance is the

anatomical tendency to remove undesirable particles from the lungs of which there are multiple mechanisms. Clearance mechanisms are important to mention because it may explain the translocation behavior of the nanoparticles following the aerosol deposition in the lungs.

Mucociliary Escalator

For the tracheobronchial region, the dominant clearance mechanism is achieved via mucociliary transport consisting of continuous, rhythmic motion of cilia on the bronchial wall epithelium. This motion transports contaminant particles upon viscous capture sustained by the mucus composed of the gel and periciliary/sol layers produced by goblet cells that lines the tracheobronchial region. This phenomenon is common known as the mucociliary escalator. Particles captured in the mucus along the airway are propelled toward the pharynx where they can be ingested and disposed of in the gastrointestinal tract. The duration of obligatory removal of particles using this clearance mechanism is on the order of hours, even less if the particles are administered at a low dosage and prove to be irritants, and possibly more if administered in high dosages.

Alveolar Macrophages

Unlike the lung airways, the alveolar regions of the lung are incapable of mucociliary transport because their sole function is to provide gas exchange with the bloodstream and pulmonary arteries. The clearance mechanism in this region is characterized by alveolar macrophages that capture particles and translocate them to the mucociliary escalator, lymphatic or venous/circulatory system. The destination of translocation is determined by the solubility of captured particles. Soluble substances can permeate the alveolar membrane where they are

translocated via the venous system. It is hypothesized that nanoparticles will qualify as soluble particle and will thus appear in the venous system. Insoluble substances are likely to be transferred to the lymphatic system and the duration of obligatory removal of these particles is on the order of months to years. Issues arise if clearance mechanisms are incapacitated. For instance, pulmonary fibrosis will occur in the case of prolonged residence of fibro-genic dusts because the alveolar macrophage capture mechanism is impaired by those substances. Particle translocation was reported using 20 nm iridium nanoparticles from the lung surface into pulmonary tissue such that they might be subject to lymphatic drainage and venous incidence thus suggesting migration to secondary organs. Some particle translocation resulting in a venous presence however small was also reported in a study using TiO2 nanoparticles. The lymphatic drainage was not assessed in this study [56, 57]. While a small number of nanoparticles were also reported for the iridium translocation (10% of those administered across the secondary organs, skeleton, and soft tissue [58]), it can be argued that the method of administration and functionalization type would affect this translocation significantly. For instance, TiO2 aerosols are generated from nanoparticles that wholly form a powder that is used for delivery. This method is in contrast to the delivery method proposed here where Au-NPs are suspended in a fluid solution that is the delivery agent to be aerosolized. The functionalization technique, if any, used for the iridium particles is not known [59].

Models

Using experimental data from research, several models have been developed to model deposition to include the Human Respiratory Tract Model from the International Commission on Radiological Protection (ICRP) and the National Council on Radiation Protection and

Measurement (NCRP). The deposition curves from these models are similar except for discrepancies in the ultrafine particle range < 1-2 pm [63]. A java-based application known as MPPD or Multiple-Path Particle Dosimetry Model performs calculations to yield an extensive amount of information regarding deposition influenced by parameters discussed previously using the HRTM models as well as characterized murine models [64].

Objectives

The objective of this research is to determine the optimal method for generation and pulmonary delivery of an aerosol that is easy and consistent. One of the first steps for optimization in rodent preclinical trials is designing the first tailored system for the pulmonary delivery of aerosols. Considerations to be taken in the design of this device are material composition, geometry, components and systematic relationships, and qualitative efficacy of the design. This optimization is intended to assist in experiments that will utilize nanoparticle aerosols as contrast agents for single or multi-modal imaging or therapeutic pulmonary delivery of radiolabeled nanoparticles to cancer sites for mitigation of metastasis. This document will detail the design considerations and results of a synthesized device as well as some specific procedures and methodologies for use of the device in select applications. However, the intent is not to limit the utilization of the device to these select applications. Rather, the future hopes it will be used more generally by revising and adapting these methodologies for any selection of applications.

CHAPTER II

DEVICE DESIGN AND FEATURES

Overview

The proposed therapeutic device possesses several features to be noted shortly. These features can be seen on the device in Figure 2 and the merit of these features and design considerations will be elaborated upon in the succeeding sections.

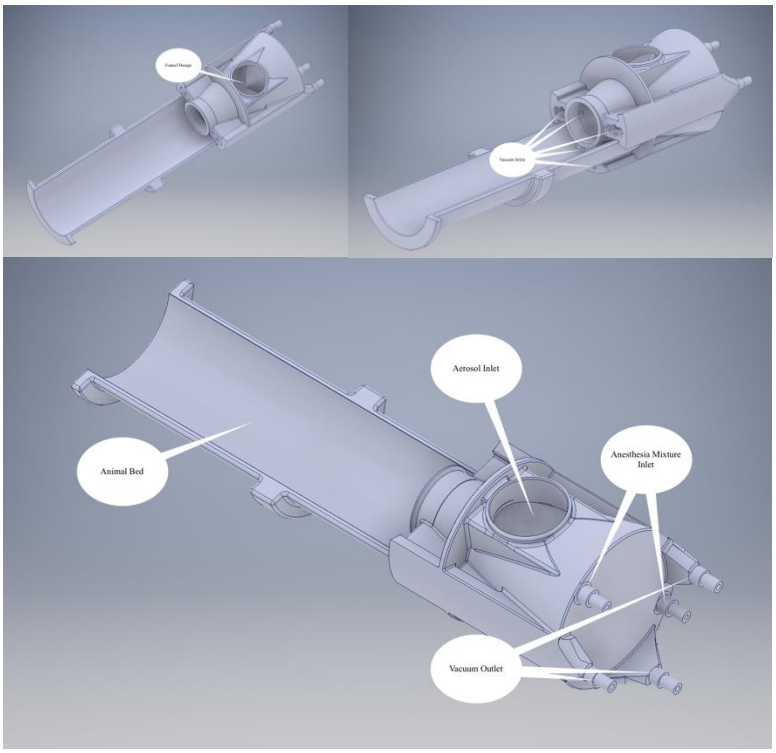

Figure 2. This figure provides a several pictures of the device with annotations.

The therapeutic device is designed with specific considerations for use within the AlbiraSi preclinical imaging machine.

Bruker AlbiraSi

The AlbiraSi is a Full Field of View multimodal PET, SPECT, CT system of high performance and MRI compatible. A diagram of the AlbiraSi is provided in Figure 3.

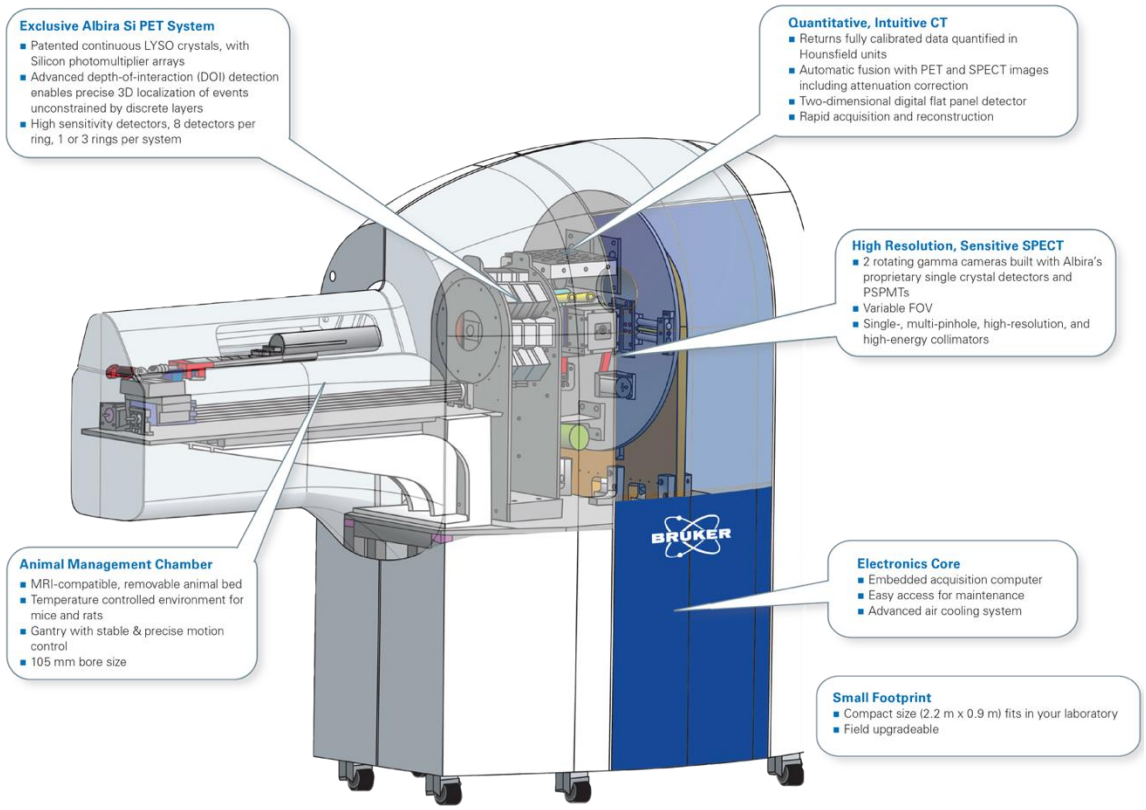

Figure 3. This figure provides a detailed diagram of the Albira with included features.

"To better understand the progression and treatment of diseases, you can use Albira's PET, SPECT and CT imaging for quantitative 3D tomographic imaging of radiotracers, bone, and soft tissue. Below are just a few of the applications of the Albira system that can provide deep insight into the underlying mechanisms of diseases and the effectiveness of new therapeutics:

- Pharmacokinetics
- Pharmacodynamics
- ADME
- Protein expression
- Metabolic studies
- Gene expression
- Toxicology
- Perfusion studies”

Some of the technical specifications of the AlbiraSi are provided in Appendix A. The therapeutic device will be managed in the “Animal Management Chamber” and then inserted into the detection chamber for imaging.

Integration

Below are figures that illustrate the integration of the system with the complete assembly in the Albira Si.

Figure 4. This figure shows the assembly of the device with vacuum and anesthesia lines connected in the rear and the AeroGen Pro mounted on top. This figure provides a detailed diagram of the device integrated into the Albira.

Atomizer

There is a wide variety of methods used to produce aerosols. The proposed design for this research assumes a piezoelectric mesh atomizer which qualifies as an ultrasonic vibrating mesh small-volume nebulizer. The device features the AeroGen Pro which contains a vibrating piezo-electric palladium mesh. “The central aperture plate is just 5mm in diameter and is perforated with 1000 precision formed holes, that vibrate at 128,000 times per second, to produce the optimum particle size for deep lung penetration.”

Figure 5. This figure provides a detailed diagram of the AeroGen Pro with included features. This figure lightly illustrates the aerosol dispersion behavior of the atomizer.

AeroGen claims a MMAD of 1-5 µm for this device and the AeroGen Pro used in the design was calibrated by AeroGen to have a MMAD of 3.7 µm. A more detailed view of the action of the atomizer is shown in Figure 5. The deposition efficiency comparison between the AeroGen Pro and traditional small volume nebulizers is illustrated in Figure 6. It can be seen from the graphic that the deposition in the lung is more ubiquitous and penetrates deeper for the

AeroGen Pro than for that of traditional SVN's. AeroGen claims that it is capable of producing lung deposition of 17% compared to a standard SVN with 3% lung deposition.

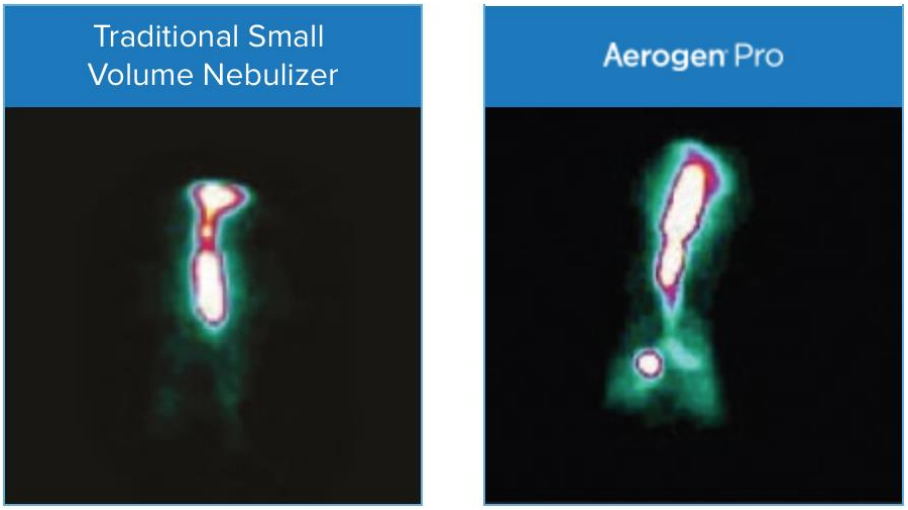

Figure 6. This figure illustrates the efficacy of deposition by the AeroGen Pro compared to traditional SVN's in the human lung.

Anesthesia System

The device features an anesthesia supply connected via the two input leads on the rear end of the device. This supply will feature a variable isoflurane-oxygen mixture. The isoflurane mixture will also serve as a mechanism to push the aerosol toward the nose of the specimen and to the vacuum. Figure 7 depicts the anesthesia system that links to the device via the leads mentioned earlier.

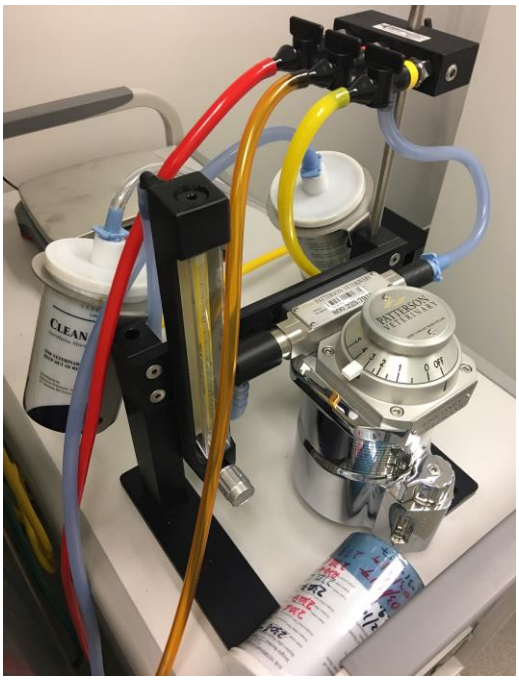

Figure 7. This figure illustrates the efficacy of deposition by the AeroGen Pro compared to traditional SVN's in the human lung.

Mixing Chamber

The mixing chamber of the device took significant consideration in the design of the geometry. Intuition mandated a funnel design that would attempt to reduce deposition, due to geometrically induced turbulence, of the aerosol on the walls of the mixing chamber. The origin of this turbulence would stem from the "hard-edge" geometry of a straight cylinder. The anesthesia system features two ports at the rear end of the device designed to "push" the aerosol through to the other end of the mixing chamber. Originally, these two ports consisted of an entire annulus with integrated blades intended to focus the aerosol to the other end of the mixing chamber. However, due to complications with the 3D printing process, the blades and annulus were abandoned. From Figure 5, it can be seen that at even a close distance from the atomizer,

the aerosol features homogeneity in terms of mist velocity and spatial particle distribution. In addition, and in contrast with jet atomizers, the generated particles seem to be less prone to coalescence and the consequent polydispersity.

Vacuum Exhaust System

The device features a vacuum exhaust system that removes the excess aerosol from the mixing chamber. In addition, the vacuum exhaust regulates the flow of the aerosol to consistently pass in front of the nose of the rodent for sustained dosage. There are multiple outlets for this vacuum system which are labeled in Figure 4. This feature is a key element in maintaining isolation of the specimen from radioactive contamination. In the event the aerosol leaks to the housing chamber with the rodent bed, the vacuum system will remove the impurities from this region though the outlets.

Figure 8. This figure portrays the vacuum system used during experimentation.

Physiological Monitoring

The BIOPAC physiological monitoring system is a feature of the Albira Si. This feature will play a large role in characterizing the breathing pattern of the rodent specimen. It consists of an air-filled, foam-like device that can expand and contract under the pressure of the body of the mouse. The pressure changes inside the device will provide readings that can be represented graphically.

Figure 9. This figure portrays the BIOPAC respiratory gating detector

Containment & Isolation System

The containment/isolation system of the therapeutic device consists of a cylindrical acrylic exterior which should be airtight and capable of displacing all radioactive aerosols from the region. Failure to maintain isolation would result contamination of the region surrounding the rodent specimen thereby rendering imaging by the Albira Si ineffective and potentially useless.

General

The device is made entirely from 3D printed VeroWhite Polyjet material. The properties of this material are detailed in Figure 10.

RIGID OPAQUE MATERIALS VEROPUREWHITE RGD837, VEROGRAY RGD850, VEROBLACKPLUS RGD875, VEROWHITEPLUS RGD835, VEROYELLOW RGD836, VEROCYAN RGD841, VEROMAGENTA RGD851					
	ASTM	UNITS	METRIC	UNITS	IMPERIAL
Tensile strength	D-638-03	MPa	50-65	psi	7250-9450
Elongation at break	D-638-05	%	10-25	%	10-25
Modulus of elasticity	D-638-04	MPa	2000-3000	psi	290,000-435,000
Flexural Strength	D-790-03	MPa	75-110	psi	11000-16000
Flexural Modulus	D-790-04	MPa	2200-3200	psi	320,000-465,000
HDT, °C @ 0.45MPa	D-648-06	°C	45-50	°F	113-122
HDT, °C @ 1.82MPa	D-648-07	°C	45-50	°F	113-122
Izod Notched Impact	D-256-06	J/m	20-30	ft lb/inch	0.375-0.562
Water Absorption	D-570-98 24hr	%	1.1-1.5	%	1.1-1.5
Tg	DMA, E»	°C	52-54	°F	126-129
Shore Hardness (D)	Scale D	Scale D	83-86	Scale D	83-86
Rockwell Hardness	Scale M	Scale M	73-76	Scale M	73-76
Polymerized density	ASTM D792	g/cm3	1.17-1.18		
Ash content VeroGray, VeroWhitePlus	USP281	%	0.23-0.26	%	0.23-0.26
Ash content VeroBlackPlus	USP281	%	0.01-0.02	%	0.01-0.02

Figure 10. This figure details the properties of the VeroWhite polyjet 3D printing material.

This material offers great resistance to fluid permeation and offers some of the highest resolution/surface finish of other 3D printing materials. The features are important considering this device is to be used with radioactive fluids and the device must not harbor any residual contamination after use. Another key feature of the device is the internalization of the airway channels for both the vacuum and anesthesia systems. This is a feature of both function and convenience. By internalizing the channels, the anesthesia can be more effectively directed to the mixing chamber to mix with the aerosolized nanoparticle solution. The device also features two cap inserts that can be removed to more effectively clean the vacuum channels.

CHAPTER III

METHODOLOGY

Fluid Dynamics

Currently, no easy simulation techniques exist to model aerosols (several advanced methods do exist for this modeling: OpenFOAM, ANSYS CFX, FLUENT) [65, 66] in the complex environment proposed here. As a result, it is difficult to model the behavior of the aerosol as it propagates through the device without extensive knowledge of the nature of aerosols and the physics that govern their behavior. Consequently, the CFD modeling of the device has been abandoned for now in spite of the valuable information it may provide regarding the internal behavior of the fluid mixture. Fortunately, this might be less of a concern at the moment if desirable results are obtained in actual experiments. Regardless, "accurate and reliable models for simulating transport, deposition, coagulation, and dispersion of nanoparticles and their aggregates are needed for the development of design tools for technological nanoparticle applications" [67].

MPPD Calculations

MPPD calculations were made for both the human and murine species in conjunction with the characterization of the device which were referenced for several determinations made in the results section.

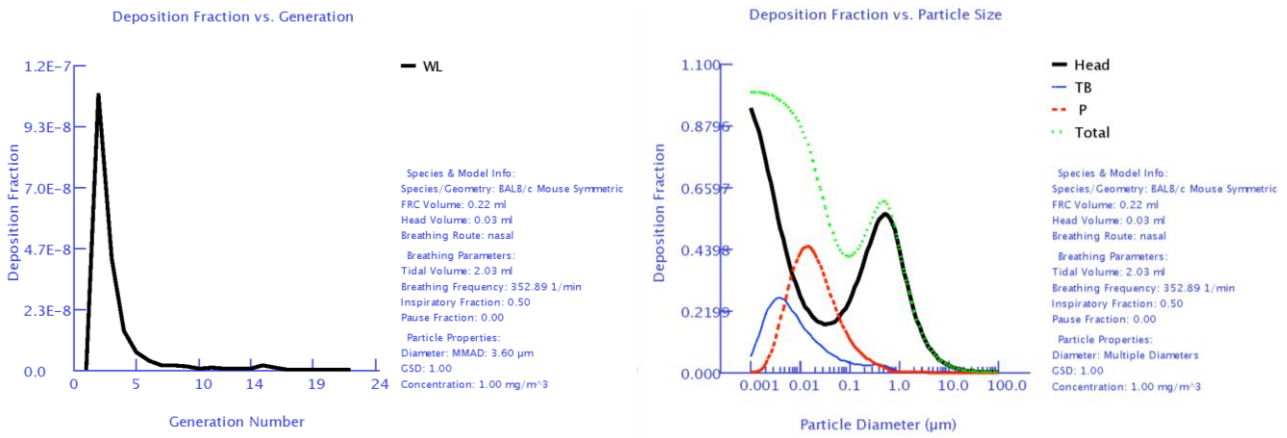

Figure 11. This figure illustrates the relationships for aerosol respiratory deposition in mice.

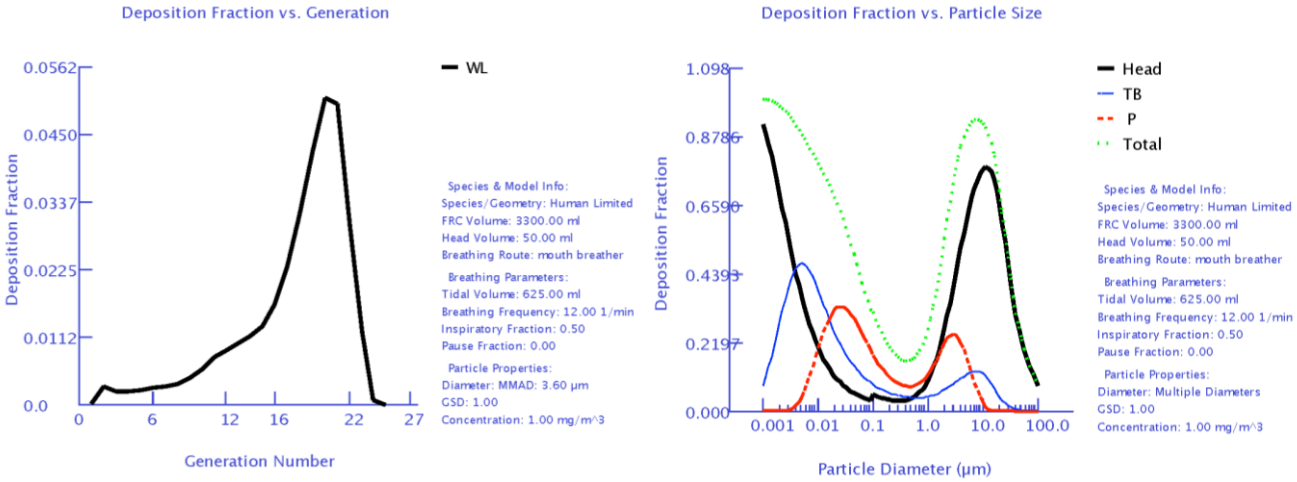

Figure 12. This figure illustrates the relationships for aerosol respiratory deposition in humans.

System Integration & Characterization

Due to lack of required qualifications, the exact procedures of the initial trial were conducted by my advisor and accompanying graduate students. As a result, the exact methodology for obtaining the results of this trial will not be detailed thoroughly. The research conducted here is intended to explicate the performance of the device first. The system was integrated and tested *in vivo* using mice models. The experiment was conducted via inhaled administration of .5 mL of FDG. Appropriate qualitative and quantitative characterizations were made regarding the atomizer, anesthesia system, vacuum exhaust system, isolation system, and physiological monitoring/data collection. The anesthesia system was controlled by and therefore characterized using the system illustrated by Figure 7. The isoflurane-oxygen ratio could be adjusted at any point using this system. The vacuum exhaust system depicted in Figure 8 allowed for the characterization of the vacuum pressure required for the removal of residual aerosol.

The isolation system was characterized using the images formed by the Albira Si imaging reconstruction. The images were assessed for radioactivity denoted by color. If any color was visible around the animal bed, the isolation system would be deemed malfunctioned because contamination would have permeated the animal housing chamber. The animal physiology monitoring was conducted using the BIOPAC monitoring system illustrated in Figure 9 and the specimen physiology was characterized thusly. The data collection produced from this monitoring provides insight into the respiratory pattern that is manifested in response to the anesthesia and otherwise.

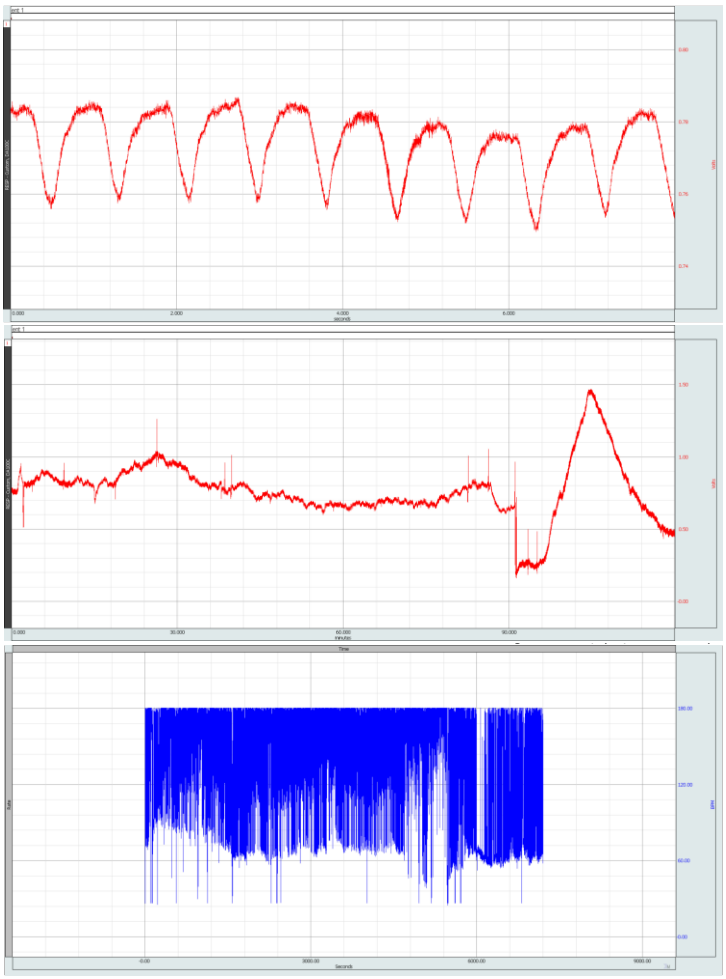

Figure 13. This figure details the breathing pattern of the mouse used in experimentation.

CHAPTER IV

RESULTS AND DISCUSSION

Upon the first trial of the therapeutic device and its integration in the Albira Si, a number of significant findings were educed and are detailed here. First, the vacuum exhaust must be sufficient enough to extract the aerosol at a rate that prevents the mouse from suffocating from a dense concentration of aerosolized FDG, although, the exact magnitude of this exhaust pressure has yet to be characterized. The MMAD of the aerosol generated by the AeroGen Pro is 3.7 μm. This particle size is much too large for distal deposition in murine specimens. Ideal particle size is around 0.01 μm as can be seen from MPPD models. It can be seen from Figure 14 that the activity inhaled by the murine specimen was incredibly low and particle deposition seemed only to occur in the nose. One speculation does exist in consideration of both the MPPD models and the features of the device itself. Some experiments reported sufficient deposition using the Aerogen Pro and not with roughly the same MMAD [68-70]. This proposes the idea that the vacuum system removes those smaller particles that would yield the desired distal deposition. It is important to note, also, that if the particles generated from the AeroGen Pro are, in fact, monodisperse, the idea aforementioned can be refuted. Finally, the radioactive tracer substance is, in fact, contained within the device so as to prevent contamination in the mouse bed which would interfere with PET/CT imaging by the Albira Si.

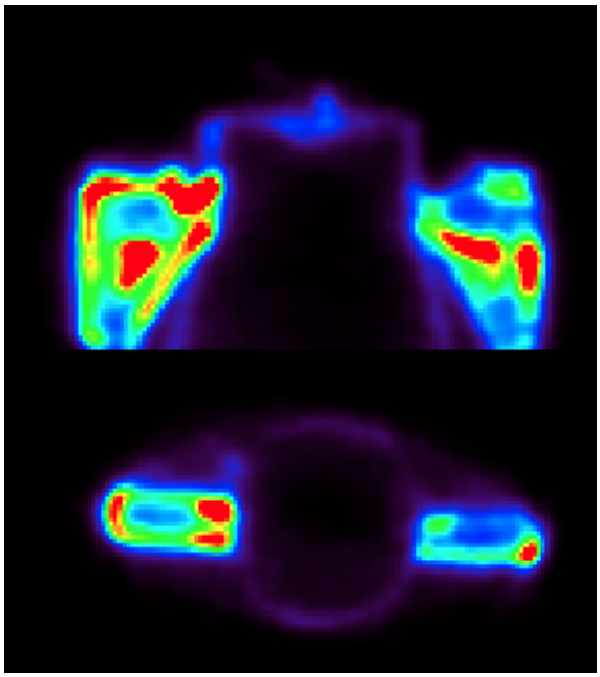

Figure 14. This figure illustrates the distribution of FDG in the device

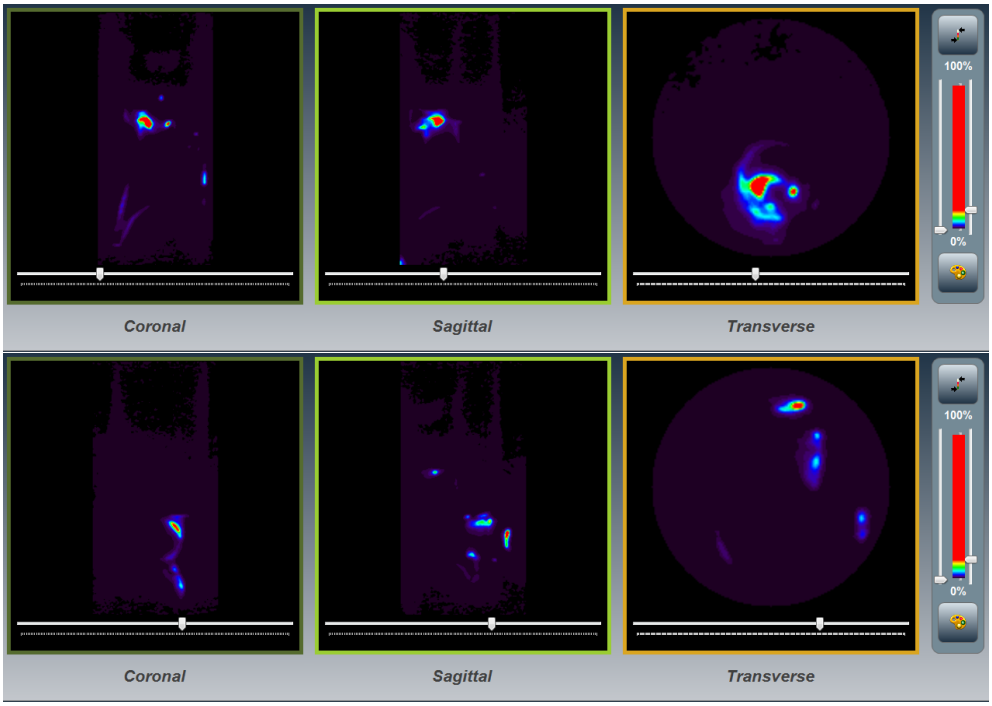

Figure 15. This figure also illustrates the distribution of FDG in the device at the denoted slice locations.

CHAPTER V

CONCLUSION

It is important to consider the long-term use of this device in regard to its current fabrication. While the absorption of fluid by the device is not projected to be an issue given the material composition, long term use may challenge this projection. If the device does absorb radioactive material, this will have serious implications regarding the function and handling of the device. The absorption will be evident and obvious in the image reconstruction performed by the Albira Si. While the device is currently a prototype, this consideration must be stated so that better material composition options can be explored to include those that are completely impermeable to fluid and transparent for monitoring of aerosol behavior within the mixing chamber. As can be seen in Figure 14, significant condensation occurs internal to the device which may affect prolonged use and efficiency. Recovery methods of condensate should be explored. Alternatively, a pulsing method for aerosol generation might prove to be a better but more difficult implementation. Currently, the Aerogen Pro features a USB controller that can adjust the treatment method between a 30 min and 6-hour dose. Ideally, this USB controller could be altered for connectivity to a computer and thereby a range of programming possibilities. If this is accomplished, two options present themselves. First, the respiratory pattern collected from the BIOPAC monitoring system can be analyzed by a computer program to determine the optimal point for pulsing of the atomizer. This would mean that in order to changing the pulsing pattern, one would need to alter the computer code. A continuous flow of the aerosol would be foremost inefficient and to attempt to match the BPM of a normal rodent would fail to account for the effect of anesthesia on the specimen and any other potential variability that might occur.

However, an even better solution would suggest the real-time evaluation of the respiratory pattern and a consequent synchronization of the atomizer pulsing. This would accomplish several things: the system would be able to account for changes in the specimen breathing pattern, the suffocation endured by the mouse would still be avoided and the vacuum system would only require activation upon absolute necessity (or run passively at a much lower vacuum pressure), the speculated effects of the vacuum removal of preferred-sized particles would be irrelevant, and the amount of aerosol administered would be dramatically reduced thus conserving the active substance and reducing the amount of condensate that resides in the mixing chamber. Due to the dramatic reduction in breathing rate accomplished by the isoflurane, the body temperature of the murine specimen also dramatically decreases. With this consideration, it might also be beneficial to explore the implementation of a heated bed to maintain the normal body temperature of the specimen.

REFERENCES

1. Van der Schee, M.P., et al., *Breathomics in lung disease.* Chest, 2015. **147**(1): p. 224-31.

2. Auletta, L., et al., *Advances in multimodal molecular imaging.* Q J Nucl Med Mol Imaging, 2017. **61**(1): p. 19-32.

3. Kiessling, F., et al., *Recent advances in molecular, multimodal and theranostic ultrasound imaging.* Adv Drug Deliv Rev, 2014. **72**: p. 15-27.

4. Martinez-Rodriguez, I. and I. Banzo, *Advances in PET: The success of multimodal molecular imaging.* Med Clin (Barc), 2017. **148**(8): p. 354-356.

5. Shaw, A.T., D.G. Kirsch, and T. Jacks, *Future of early detection of lung cancer: the role of mouse models.* Clin Cancer Res, 2005. **11**(13 Pt 2): p. 4999s-5003s.

6. Garrastazu Pereira, G., et al., *Loco-regional administration of nanomedicines for the treatment of lung cancer.* Drug Deliv, 2016. **23**(8): p. 2881-2896.

7. Hussain, S., *Nanomedicine for Treatment of Lung Cancer.* Adv Exp Med Biol, 2016. **890**: p. 137-47.

8. Anchordoquy, T.J., et al., *Mechanisms and Barriers in Cancer Nanomedicine: Addressing Challenges, Looking for Solutions.* ACS Nano, 2017. **11**(1): p. 12-18.

9. Landesman-Milo, D., S. Ramishetti, and D. Peer, *Nanomedicine as an emerging platform for metastatic lung cancer therapy.* Cancer Metastasis Rev, 2015. **34**(2): p. 291-301.

10. Shete, H.K., et al., *Pulmonary multifunctional nano-oncological modules for lung cancer treatment and prevention.* J Biomed Nanotechnol, 2014. **10**(9): p. 1863-93.

11. Iyer, R., C.C. Hsia, and K.T. Nguyen, *Nano-Therapeutics for the Lung: State-of-the-Art and Future Perspectives.* Curr Pharm Des, 2015. **21**(36): p. 5233-44.

12. Muralidharan, P., et al., *Inhalable nanoparticulate powders for respiratory delivery.* Nanomedicine, 2015. **11**(5): p. 1189-99.

13. Mortensen, N.P. and A.J. Hickey, *Targeting inhaled therapy beyond the lungs.* Respiration, 2014. **88**(5): p. 353-4.

14. Loira-Pastoriza, C., J. Todoroff, and R. Vanbever, *Delivery strategies for sustained drug release in the lungs.* Adv Drug Deliv Rev, 2014. **75**: p. 81-91.

15. Darquenne, C., et al., *Bridging the Gap Between Science and Clinical Efficacy: Physiology, Imaging, and Modeling of Aerosols in the Lung.* J Aerosol Med Pulm Drug Deliv, 2016. **29**(2): p. 107-26.

16. Jacob, B., B.R. O'Driscoll, and J.H. Dennis, *Practical Handbook of Nebulizer Therapy*. 2003: Taylor & Francis.

17. Mitchell, J.P., J. Suggett, and M. Nagel, *Clinically Relevant In Vitro Testing of Orally Inhaled Products-Bridging the Gap Between the Lab and the Patient.* AAPS PharmSciTech, 2016. **17**(4): p. 787-804.

18. Dyawanapelly, S., A. Kumar, and M.K. Chourasia, *Lessons Learned from Gemcitabine: Impact of Therapeutic Carrier Systems and Gemcitabine's Drug Conjugates on Cancer Therapy.* Crit Rev Ther Drug Carrier Syst, 2017. **34**(1): p. 63-96.

19. Food and Drug Administration, *Guidance for Industry: Considering Whether an FDA-Regulated Product Involves the Application of Nanotechnology*. 2014, FDA Maryland.

20. Libutti, S.K., et al., *Phase I and pharmacokinetic studies of CYT-6091, a novel PEGylated colloidal gold-rhTNF nanomedicine.* Clin Cancer Res, 2010. **16**(24): p. 6139-49.

21. Paciotti, G.F., et al., *Colloidal gold: a novel nanoparticle vector for tumor directed drug delivery.* Drug Deliv, 2004. **11**(3): p. 169-83.

22. Eslamian, M. and N. Ashgriz, *Swirl, T-Jet and Vibrating-Mesh Atomizers*, in *Handbook of Atomization and Sprays: Theory and Applications*, N. Ashgriz, Editor. 2011, Springer US: Boston, MA. p. 755-773.

23. Arı, A., *Jet, Ultrasonic, and Mesh Nebulizers: An Evaluation of Nebulizers for Better Clinical Outcomes.* Eurasian Journal of Pulmonology, 2014. **16**(1): p. 1-7.

24. Ari, A., et al., *Influence of nebulizer type, position, and bias flow on aerosol drug delivery in simulated pediatric and adult lung models during mechanical ventilation.* Respir Care, 2010. **55**(7): p. 845-51.

25. Ari, A. and J.B. Fink, *Breath-actuated nebulizer versus small-volume nebulizer: efficacy, safety, and satisfaction.* Respir Care, 2012. **57**(8): p. 1351-3.

26. Rau, J.L., A. Ari, and R.D. Restrepo, *Performance comparison of nebulizer designs: constant-output, breath-enhanced, and dosimetric.* Respir Care, 2004. **49**(2): p. 174-9.

27. Dhand, R., *Nebulizers that use a vibrating mesh or plate with multiple apertures to generate aerosol.* Respir Care, 2002. **47**(12): p. 1406-16; discussion 1416-8.

28. Yang, W., J.I. Peters, and R.O. Williams, 3rd, *Inhaled nanoparticles--a current review.* Int J Pharm, 2008. **356**(1-2): p. 239-47.

29. Cook, M.J., *The anatomy of the laboratory mouse*. 1965: London ; New York : Academic Press, 1965.

30. Mendez, L.B., G. Gookin, and R.F. Phalen, *Inhaled aerosol particle dosimetry in mice: a review.* Inhal Toxicol, 2010. **22 Suppl 2**: p. 15-20.

31. Irvin, C.G. and J.H. Bates, *Measuring the lung function in the mouse: the challenge of size.* Respir Res, 2003. **4**: p. 4.

32. Bennett, F.M. and S.M. Tenney, *Comparative mechanics of mammalian respiratory system.* Respir Physiol, 1982. **49**(2): p. 131-40.

33. Braakhuis, H.M., et al., *Progress and future of in vitro models to study translocation of nanoparticles.* Arch Toxicol, 2015. **89**(9): p. 1469-95.

34. Gomes, R.F. and J.H. Bates, *Geometric determinants of airway resistance in two isomorphic rodent species.* Respir Physiol Neurobiol, 2002. **130**(3): p. 317-25.

35. Innes, B.A. and J.R. Dorin, *Submucosal gland distribution in the mouse has a genetic determination localized on chromosome 9.* Mamm Genome, 2001. **12**(2): p. 124-8.

36. Reynolds, S.D. and A.M. Malkinson, *Clara cell: progenitor for the bronchiolar epithelium.* Int J Biochem Cell Biol, 2010. **42**(1): p. 1-4.

37. Meuwissen, R. and A. Berns, *Mouse models for human lung cancer.* Genes Dev, 2005. **19**(6): p. 643-64.

38. Kellar, A., C. Egan, and D. Morris, *Preclinical Murine Models for Lung Cancer: Clinical Trial Applications.* Biomed Res Int, 2015. **2015**: p. 621324.

39. Vandamme, T.F., *Use of rodents as models of human diseases.* J Pharm Bioallied Sci, 2014. **6**(1): p. 2-9.

40. Kimling, J., et al., *Turkevich method for gold nanoparticle synthesis revisited.* J Phys Chem B, 2006. **110**(32): p. 15700-7.

41. Perala, S.R. and S. Kumar, *On the mechanism of metal nanoparticle synthesis in the Brust-Schiffrin method.* Langmuir, 2013. **29**(31): p. 9863-73.

42. Deraedt, C., et al., *Sodium borohydride stabilizes very active gold nanoparticle catalysts.* Chem Commun (Camb), 2014. **50**(91): p. 14194-6.

43. Sakai, T., et al., *Hydrogen-assisted fabrication of spherical gold nanoparticles through sonochemical reduction of tetrachloride gold(III) ions in water.* Ultrason Sonochem, 2014. **21**(3): p. 946-50.

44. Zhou, J., et al., *Functionalized gold nanoparticles: synthesis, structure and colloid stability.* J Colloid Interface Sci, 2009. **331**(2): p. 251-62.

45. Chanda, N., et al., *Radioactive gold nanoparticles in cancer therapy: therapeutic efficacy studies of GA-198AuNP nanoconstruct in prostate tumor-bearing mice.* Nanomedicine, 2010. **6**(2): p. 201-9.

46. van Vlerken, L.E., T.K. Vyas, and M.M. Amiji, *Poly(ethylene glycol)-modified nanocarriers for tumor-targeted and intracellular delivery.* Pharm Res, 2007. **24**(8): p. 1405-14.

47. Jokerst, J.V., et al., *Nanoparticle PEGylation for imaging and therapy.* Nanomedicine (Lond), 2011. **6**(4): p. 715-28.

48. Möller, W., et al., *Gold nanoparticle aerosols for rodent inhalation and translocation studies.* Journal of Nanoparticle Research, 2013. **15**(4): p. 1574.

49. Choi, C.H., et al., *Mechanism of active targeting in solid tumors with transferrin-containing gold nanoparticles.* Proc Natl Acad Sci U S A, 2010. **107**(3): p. 1235-40.

50. Liberman, A., et al., *Synthesis and surface functionalization of silica nanoparticles for nanomedicine.* Surf Sci Rep, 2014. **69**(2-3): p. 132-158.

51. Mout, R., et al., *Surface functionalization of nanoparticles for nanomedicine.* Chem Soc Rev, 2012. **41**(7): p. 2539-44.

52. Lin, L., et al., *SLC transporters as therapeutic targets: emerging opportunities.* Nat Rev Drug Discov, 2015. **14**(8): p. 543-60.

53. Nakanishi, T., *Drug transporters as targets for cancer chemotherapy.* Cancer Genomics Proteomics, 2007. **4**(3): p. 241-54.

54. Weber, E. and H.J. Ehrlein, *Glucose and maltodextrin in enteral diets have different effects on jejunal absorption of nutrients, sodium and water and on flow rate in mini pigs.* Dtsch Tierarztl Wochenschr, 1998. **105**(12): p. 446-9.

55. Abbas, Y., et al., *Development of an inhalable, stimuli-responsive particulate system for delivery to deep lung tissue.* Colloids Surf B Biointerfaces, 2016. **146**: p. 19-30.

56. Semmler, M., et al., *Long-term clearance kinetics of inhaled ultrafine insoluble iridium particles from the rat lung, including transient translocation into secondary organs.* Inhal Toxicol, 2004. **16**(6-7): p. 453-9.

57. Semmler-Behnke, M., et al., *Efficient elimination of inhaled nanoparticles from the alveolar region: evidence for interstitial uptake and subsequent reentrainment onto airways epithelium.* Environ Health Perspect, 2007. **115**(5): p. 728-33.

58. Kreyling, W.G., et al., *Size dependence of the translocation of inhaled iridium and carbon nanoparticle aggregates from the lung of rats to the blood and secondary target organs.* Inhal Toxicol, 2009. **21 Suppl 1**: p. 55-60.

59. Geiser, M. and W.G. Kreyling, *Deposition and biokinetics of inhaled nanoparticles.* Part Fibre Toxicol, 2010. **7**: p. 2.

60. Fritsch, P., *Uncertainties in aerosol deposition within the respiratory tract using the icrp 66 model: a study in workers.* Health Phys, 2006. **90**(2): p. 114-26.

61. Harley, N.H., I.M. Fisenne, and E.S. Robbins, *Attempted validation of ICRP 30 and ICRP 66 respiratory models.* Radiat Prot Dosimetry, 2012. **152**(1-3): p. 14-7.

62. Harvey, R.P. and D.M. Hamby, *Age-specific uncertainty in particulate deposition for 1 microm AMAD particles using the ICRP 66 lung model.* Health Phys, 2002. **82**(6): p. 807-16.

63. Yeh, H.-C., et al., *Comparisons of Calculated Respiratory Tract Deposition of Particles Based on the Proposed NCRP Model and the New ICRP66 Model.* Aerosol Science and Technology, 1996. **25**(2): p. 134-140.

64. Anjilvel, S. and B. Asgharian, *A multiple-path model of particle deposition in the rat lung.* Fundam Appl Toxicol, 1995. **28**(1): p. 41-50.

65. Nowak, N., Kakade, P.P. & Annapragada, A.V. Annals of Biomedical Engineering (2003) 31: 374. doi:10.1114/1.1560632

66. Pyyk önen, Jouni, and Jorma Jokiniemi. “Computational Fluid Dynamics Based Sectional Aerosol Modelling Schemes.” Journal of Aerosol Science 31, no. 5 (2000): 531–50.

67. Friedlander, Sheldon K., and David Y.h. Pui. "Emerging Issues in Nanoparticle Aerosol Science and Technology." Journal of Nanoparticle Research 6.2/3 (2004): 313-20. Web.

68. Hindi, Khadijah M, Andrew J Ditto, Matthew J Panzner, Douglas A Medvetz, Daniel S Han, Christine E Hovis, Julia K Hilliard, et al. *The Antimicrobial Efficacy of Sustained Release Silver–Carbene Complex-Loaded L-Tyrosine Polyphosphate Nanoparticles: Characterization, in Vitro and in Vivo Studies.* Biomaterials 30, no. 22 (n.d.): 3771–79.

69. Shvedova, Anna A, Elena R Kisin, Robert Mercer, Ashley R Murray, Victor J Johnson, Alla I Potapovich, Yulia Y Tyurina, et al. *Unusual Inflammatory and Fibrogenic Pulmonary Responses to Single-Walled Carbon Nanotubes in Mice...* AJP: Lung Cellular and Molecular Physiology 289, no. 5 (November 2005): L698–708. doi:10.1152/ajplung.00084.2005.

70. Muhle, H, and B Bellmann. *Pulmonary Clearance of Inhaled Particles in Dependence of Particle Size.* Journal of Aerosol Science 17, no. 3 (1986): 346–49.

APPENDIX A

ALBIRA SI SPECIFICATIONS

Full Field Accuracy (FFA)

FFA offers real, homogeneous sub-millimetric volumetric PET resolution in all three axes in the whole field of view, with superior precision in quantification based on: Exclusive continuous crystal detectors with new Si PM technology and true depth of interaction 3D precision equivalent to 10+ layer pixelated crystal detectors.

Virtual pixels optimizing very fast, low dose, maximum sensitivity studies and allowing software based performance upgrades Proprietary electronics and software with row and column readout, enabling advanced depth-of-interaction measurement and correction.

This patented technology generates an area of optimum resolution up to 10 times larger than conventional options.

System Specifications

- Imaging Modalities: PET, SPECT, CT
- Core Technologies: Patented continuous crystal technology with Row And Column readout + proprietary electronics + HR 3D DOI
- Unit Size: Single compact footprint
- Shielding: Fully Shielded
- Weight: 800 kg
- Bore Size: 105

Animal Care Monitoring And Control

- Anesthesia: Fully integrated. Compatible with most common commercial gas systems
- Animal Handling System: Reliable, easy to use rat and mouse beds; Fully compatible with BRUKER MR
- Physiological Signals: ECG, Respiration, Temperature, And Blood Pressure
- Temperature Control System: Electrically heated mats for rat And mouse
- Video Monitoring: Real-time camera
- Gating Acquisition: Cardiac and Respiratory For PET and SPECT; Dual Gating for PET

Software And Workstation

- Fully Integrated Albira Suite: ACQUIRER: Image Acquisition, RECONSTRUCTOR: Image Reconstruction, MANAGER: Study and Protocol Management, SUPERVISOR: Quality Control
- Image Analysis Software: PMOD (PBAS, PFUS, PKIN MODULES INCLUDED)
- 3D Rendering Software: VOLVIEW (+ PMOD)
- Workstation: Dedicated Server; All Functionalities on a single system
- Reconstruction: GPU Based, Scalable To 4 GPUs (PET); CPU Based SPECT and CT
- Data Storage: 3 * 4TB RAID 5 Configuration; Upgradable on same Workstation

PET System 3 Ring

- Module Architecture: 24 Modules, 8 modules per ring; Patented continous crystal coupled to 12x12 SiPM; Propietary electronics optimized for HR 3D DoI;
- Spatial Resolution: Up to 0,7 mm; Guaranteed submilimetric volumetric resolution; FULL FIELD ACCURACY: Homogeneous resolution better than 1,2 mm in the whole FoV of 80+ mm;
- Axial FOV: 148 mm
- Transaxial FOV: 80 mm
- Sensitivity: 12%; 9% NEMA
- Average Energy Resolution: 17%
- Reconstruction Algorithm: MLEM, Ultra fast GPU based
- Sensitivity: 9%
- NECR Mouse: Peak: 560 kcps at 35 MBq
- NECR Rat: Peak: 330 kcps at 43 MBq

PET System 1 Ring

- Module Architecture: 8 Modules in 1 ring configuration; Patented continous crystal coupled to 12x12 SiPM; Propietary electronics optimized for HR 3D DoI
- Spatial Resolution: Up to 0,7 mm[1]; Guaranteed submilimetric volumetric resolution; FULL FIELD ACCURACY: Homogeneous resolution better than 1,2 mm in the whole FoV of 80+ mm
- Axial FOV: 46 mm
- Transaxial FOV: 80 mm
- Sensitivity: 4,5%; 3% NEMA
- Average Energy Resolution: 17%
- Reconstruction Algorithm: MLEM, Ultra fast GPU based
- NECR Mouse: Peak: 80 kcps at 35 MBq
- NECR Rat: Peak: 20 kcps at 43 MBq

CT Specifications

- X RAY ENERGY: 10 – 50 kVp
- detector: Digital flat panel 2400x2400 pixels
- SPATIAL RESOLUTION: 90 um
- MAXIMUM CURRENT: 1 mA
- FOV: 70x70 mm

SPECT 108 Specifications

- DETECTOR: Dual head camera system with patented continous CsI(Na) crystal technology
- SENSITIVITY: 1.800 cps/MBq
- ENERGY RESOLUTION: 0,18
- ENERGY RANGE: 30 – 400 keV
- VARIABLE FOV: 25 – 120 mm
- SPATIAL RESOLUTION: 0.5 mm
- COLLIMATORS: A.General Purpose; B. High Energy; C. High Resolution; D. Multipinhole;
- RECONSTRUCTION: OSEM, Fast Reconstruction

Best in class specifications under real lab conditions

- Resolution up to 0.7 mm
- Sensitivity of 12%
- NEMA NECR peak rates: mouse 560 kcps, rat 330 kcps
- Unprecedented quantification and dynamic study performance
- Large axial FOV of 148 mm
- Cardiac and respiratory gating